A Circulating-Current Suppression Method for Parallel-Connected Voltage-Source Inverters With Common DC and AC Buses

Wei, Baoze; Guerrero, Josep M.; Quintero, Juan Carlos Vasquez; Guo, Xiaoqiang

Published in:
I E E E Transactions on Industry Applications

DOI (link to publication from Publisher):
10.1109/TIA.2017.2681620

Publication date:
2017

Document Version
Early version, also known as pre-print

A Circulating-Current Suppression Method for Parallel Connected Voltage Source Inverters (VSI) with Common DC and AC Buses

Baoze Wei, Josep M. Guerrero
Juan C. Vásquez
Student Member, Fellow, Senior Member, IEEE
Aalborg University
101 Pontoppidanstaede
Aalborg, 9220, Denmark
bao@et.aau.dk, joz@et.aau.dk, juq@et.aau.dk

Xiaoqiang Guo
Senior Member, IEEE
Yanshan University
438 Hebei Street
Qinhuangdao, 066004, China
gxq@ysu.edu.cn

***Abstract*—This paper presents a theoretical study with experimental validation of a circulating-current suppression method for parallel operation of three-phase voltage source inverters (VSI), which may be suitable for modular parallel uninterruptible power supply systems or hybrid AC/DC microgrid applications. The basic concept of the proposed circulating-current suppression method is to modify the original current references by using the current difference among the parallel inverters. In the proposed approach, both of cross circulating-current and zero-sequence circulating-current are considered, and added into the conventional droop plus virtual impedance control. In the control architecture, the reference voltages of the inverters are generated by the primary control loop which consists of a droop control and a virtual impedance. The secondary control is used to compensate the voltage drop on the virtual impedance. Further, a circulating-current control loop is added to improve the average current-sharing performance among parallel VSIs. Experimental results are presented to show the effectiveness of the proposed control method to suppress both of the cross and zero-sequence circulating-currents.**

***Keywords*—voltage source inverter; parallel connected; cross circulating-current; zero-sequence; common DC and AC buses**

I. INTRODUCTION

The inverters are commonly used in power converter based applications, such as the uninterruptible power systems (UPS), distributed generation (DG) systems, or microgrids [1]–[5]. In case of high power demand, it is difficult to deliver large amount of power with a single inverter since that the power rating of the switching devices is often limited or constrained by technical and/or economic considerations [6]. In order to achieve high power level of a converter system, but without increasing the current stress of the switching devices, power architectures based on parallel-connected inverters are often adopted [7]–[12]. The parallel operation also allows realizing modular design, thus decreasing the production time of the distributed power system [13]–[15]. Fig. 1 shows the power architecture consisting of two parallel-connected three-phase two-level inverters.

One of the main problems for a parallel system is the circulating-current among the inverters [16]–[19]. The circulating-current can be caused by the difference between the parameters of the parallel inverters, such as filters, switching frequency, dead-times, and the tolerances and drifts of the hardware components, etc. [6], [16], [17]. Furthermore, when the inverters are parallel-connected with both common DC and AC buses, the zero-sequence circulating-current problem should be considered together with the cross circulating-current [8], [17]. The existing circulating-currents may cause output currents distortion, increase of the voltage total harmonic distortion (THD), power losses, decrease of the power density and system efficiency, and result in different current stress of the switching devices. Furthermore, the high-frequency content of the circulating-current may lead to a serious problem of electromagnetic interference (EMI) [20], [21]. Consequently, it is necessary to develop effective methods to suppress circulating-currents, thus realizing precise average current-sharing among the parallel inverters.

A traditional method to eliminate the circulating-current problem is to add isolation transformers at the output of the inverters, thus obtaining an open circuit for the circulating-current [19]. However, transformers usually work in low frequency thus having large volume, being bulky and expensive. They may also suffer from both core and copper losses, which will decrease the efficiency and power density of the system [19].

Another way of suppressing the circulating-current is to use proper control methods [22], [23]. A traditional solution to achieve average current sharing is the frequency and voltage droop control method, which has the feature of wireless control among parallel inverters [24]. However, the performance of the droop method is particularly sensitive to the output impedance of the parallel units [25]. To overcome this problem, by using a virtual impedance loop, the output impedance of the inverters can be modified to acquire lower circulating-current with better current sharing performance [26]. The output impedance of the inverter system is related with the power plant. However, in a practical paralleled inverters system, it is not easy to get accurate hardware parameters, and some of them will drift under different operating conditions, such as temperature, humidity, and so on. Thus it is difficult to design properly the virtual impedance loop, which if poorly designed or implemented, it may introduce current distortion and may adversely affect the system dynamics and stability [27].

In order to solve the problems of the abovementioned circulating-current suppression strategies, this paper proposes a control method which is inserted into the conventional droop plus virtual impedance control to improve the current sharing

performance, and it is expanded from our previous work in [28], [29].

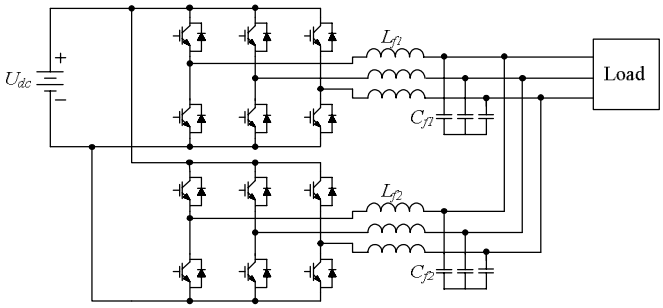

Fig. 1. Power architecture based on two parallel-connected inverters.

In the droop plus virtual impedance control, the droop is used to generate the reference voltages of each inverter. The virtual impedance is used to regulate the output impedance of the inverters. The proposed circulating-current control loops are added to assess the current difference between parallel inverters, including d-axis, q-axis and zero-axis currents, thus the current errors are used to compensate the local reference currents [29]. With proper controller design, both of the zero-sequence and the cross circulating-currents can be effectively suppressed. Thus the objective of accurate average current sharing among parallel inverters can be reached.

The basic concept of the proposed strategy is based on a distributed control scheme. In the distributed control strategy, the average unit current can be determined by measuring the total load current and then divide this current by the number of units (inverters) in the system [28], [30]. With the analysis and experimental results presented in this paper, it will be shown that the circulating-current suppression method used in this paper does not only work with current source inverter (CSI) based applications as in [28], but also with voltage source inverter (VSI) based applications. Furthermore, this paper also expands the cross circulating-current suppression to both of cross and zero-sequence circulating-currents suppression. More details will be introduced in Section II.

This paper is organized as follows. In Section II, the circulating-current analysis for parallel VSIs is discussed. The proposed control strategy based on circulating-current control loops is presented with conventional droop plus virtual impedance control. In Section III, the stability analysis is presented to discuss the influence of the added circulating-current control loops to the output voltage control of the inverters. In Section IV, experimental results are compared with conventional droop plus virtual impedance control to verify the effectiveness of the proposed method. The conclusion is given in Section V.

II. Proposed Control Strategy

A. Analysis of the Circulating-current

This paper considers a system of two parallel connected three-phase VSIs working in island mode as an example to analyze the circulating-current phenomenon. As mentioned above, circulating-currents can be classified into cross-circulating-current and zero-sequence circulating-current, which will flow from one inverter to another through the common AC and DC buses [8], [17]. This problem is particularly important for applications like AC-DC hybrid microgrids and modular parallel UPS systems.

Fig. 2 depicts the circulating-current phenomena. On the one hand, Fig. 2(a) shows the possible zero-sequence circulating-current paths. On the other hand, Fig. 2(b) shows the possible cross circulating-current paths based on different switching states. The simplified equivalent circuit of the two parallel connected inverters system is shown in Fig. 3.

According to [31], the cross circulating-current I_{cir} can be defined as

$$I_{cir} = (I_1 - I_2)/2 \tag{1}$$

being I_1 and I_2 are the output currents of the parallel inverters. Considering the output impedances of the parallel inverters Z_1 and Z_2, the I_{cir} can be calculated as

$$I_{cir} = \frac{1}{2}\left(\frac{E_1}{Z_1} - \frac{E_2}{Z_2}\right) \tag{2}$$

being E_1 and E_2 are the output voltages of the two inverters. If assuming that the output impedances are equal to each other, Z_1=Z_2=Z, then the cross circulating-current can be calculated as

$$I_{cir} = (E_1 - E_2)/2Z\,. \tag{3}$$

But as discussed in Section I, in a practical system, it is difficult to guaranty that the output impedances of the inverters are equal to each other because of different parameters of the power plants or working conditions. By using a virtual impedance loop, the cross circulating-current can be calculated as

$$I_{cir} = \frac{1}{2}\left(\frac{E_1}{Z_1 + Z_{vir1}} - \frac{E_2}{Z_2 + Z_{vir2}}\right) \tag{4}$$

being Z_{vir1} and Z_{vir2} are the virtual impedances of the two inverters respectively. The zero-sequence current I_z can be calculated as

$$I_z = (I_a + I_b + I_c)/3 \tag{5}$$

where I_a, I_b and I_c are the three phase output currents of the inverter [8], [20], then the zero-sequence circulating-current among two inverters can be obtained as following

$$I_{zcir} = (I_{z1} - I_{z2})/2\,. \tag{6}$$

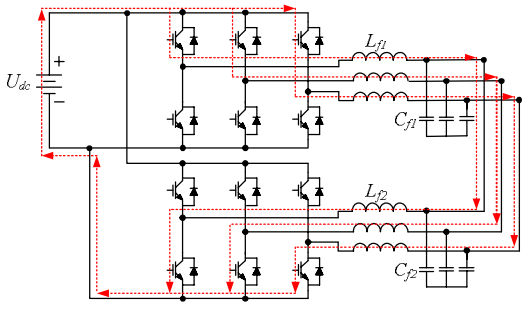

(a)

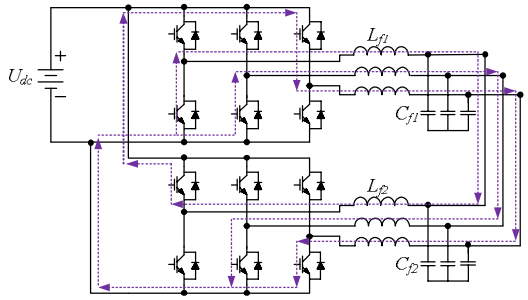

(b)

Fig. 2. Circulating-current paths. (a) Zero-sequence circulating-current. (b) Cross circulating-current.

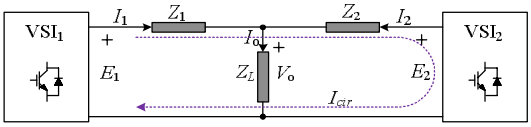

Fig. 3. Equivalent circuit of two parallel connected inverters.

B. Proposed Control Method

Fig. 4 shows the control scheme for one of the parallel units of the two parallel connected inverters system. The other one inverter will use the same control principle. The zero-sequence current of the inverter can be easily calculated by using the *abc*/*dqz* transformation of the inductor currents. Equation (7) is used to complete the transformation from stationary coordinates to synchronous rotating coordinates. Then with (6), the zero-sequence circulating-current among the inverters can be calculated.

The control scheme contains the conventional droop plus virtual impedance control, secondary control, the proposed circulating-current control loops, and the basic voltage/current control loops. In which, the droop control is responsible to generate the reference voltages for the voltage control loop, the virtual impedance is applied to obtain a similar output impedances of the parallel inverters, and the secondary control is added into the control scheme to recover the voltage drop on the virtual impedances. In Fig. 4, R_{V1} and L_{V1} are the virtual resistor and virtual inductor respectively. The basic concept of the proposed circulating-current control is to appropriately revise the reference currents which are generated by the voltage control loop. The original current references are added with the current errors among the two parallel inverters, including d-axis, q-axis and zero-axis currents. Then, new reference currents can be generated with this compensation. Finally, the switching signals are generated by using the conventional Sinusoidal Pulse Width Modulation (SPWM) method which is commonly used for the three-phase two level inverter based applications [32], [33].

$$\begin{bmatrix} i_d \\ i_q \\ i_z \end{bmatrix} = \begin{bmatrix} \cos\theta & \cos(\theta-\frac{2\pi}{3}) & \cos(\theta+\frac{2\pi}{3}) \\ -\sin\theta & -\sin(\theta-\frac{2\pi}{3}) & -\sin(\theta+\frac{2\pi}{3}) \\ \frac{1}{2} & \frac{1}{2} & \frac{1}{2} \end{bmatrix} \bullet \begin{bmatrix} i_a \\ i_b \\ i_c \end{bmatrix} \bullet \frac{2}{3} \quad (7)$$

The detailed process of generating new current references with the proposed circulating current control loops is shown as follows (8) – (19), including the d-axis, q-axis and zero-axis.

$$\left\{[0-(I_{d1}-I_{d2})]/2\right\}\bullet G_{cd1} = I_{de1} \quad (8)$$

$$\left\{[0-(I_{q1}-I_{q2})]/2\right\}\bullet G_{cq1} = I_{qe1} \quad (9)$$

$$\left\{[0-(I_{d2}-I_{d1})]/2\right\}\bullet G_{cd2} = I_{de2} \quad (10)$$

$$\left\{[0-(I_{q2}-I_{q1})]/2\right\}\bullet G_{cq2} = I_{qe2} \quad (11)$$

$$\left\{[0-(I_{z1}-I_{z2})]/2\right\}\bullet G_{cz1} = I_{ze1} \quad (12)$$

$$\left\{[0-(I_{z2}-I_{z1})]/2\right\}\bullet G_{cz2} = I_{ze2} \quad (13)$$

$$I_{dr1} + I_{de1} = I_{dr1}^{*} \quad (14)$$

$$I_{qr1} + I_{qe1} = I_{qr1}^{*} \quad (15)$$

$$I_{dr2} + I_{de2} = I_{dr2}^{*} \quad (16)$$

$$I_{qr2} + I_{qe2} = I_{qr2}^{*} \quad (17)$$

$$I_{zr1} + I_{ze1} = I_{zr1}^{*} \quad (18)$$

$$I_{zr2} + I_{ze2} = I_{zr2}^{*} \quad (19)$$

Taking the generation of d-axis reference current I_{drx}* for example, then I_{qrx}* and I_{zrx}* will use the same principle (x=1, 2). After the *abc/dqz* transformation of the currents I_{L1} and I_{L2} for VSI_1 and VSI_2, one can obtain the d-axis currents I_{d1} and I_{d2}. With (8), the d-axis compensation current I_{de1} for VSI_1 is obtained. Note that this calculation is completed in the controller of VSI_1, so that I_{d1} is in the position of minuend in (8). In (8), the difference between I_{d1} and I_{d2} will be compared with 0. The purpose of doing this is to decide the compensation direction, increasing or decreasing the reference currents. Another consideration is that "0" is like a reference value because the compensation currents should be 0 if there is no circulating-current. The gain "1/2" is used in this particular case to calculate the cross circulating-current from (1). G_{cd1} is the controller in the d-axis circulating-current control loop. Then, by substituting (8) into (14), one can obtain the new reference current I_{dr1}* for the VSI_1. Being I_{dr1} is the original d-axis reference current.

To explain the functions more clearly, supposing that the currents $I_{d1}>I_{d2}$, the correct direction of the compensation should be decreasing reference I_{dr1} for VSI_1 and increasing I_{dr2} for VSI_2. The calculation results from (8) and (10) will be $I_{de1}<0$, $I_{de2}>0$. Substituting (8) into (14), and (10) into (16), the new d-axis reference current I_{dr1}* will be subtracted from I_{dr1}, and I_{dr2}* will be increased from I_{dr2}, which indicates the correct compensation direction. So that, with proper design of the circulating-current controllers, the cross and the zero-sequence circulating-currents can be effectively suppressed.

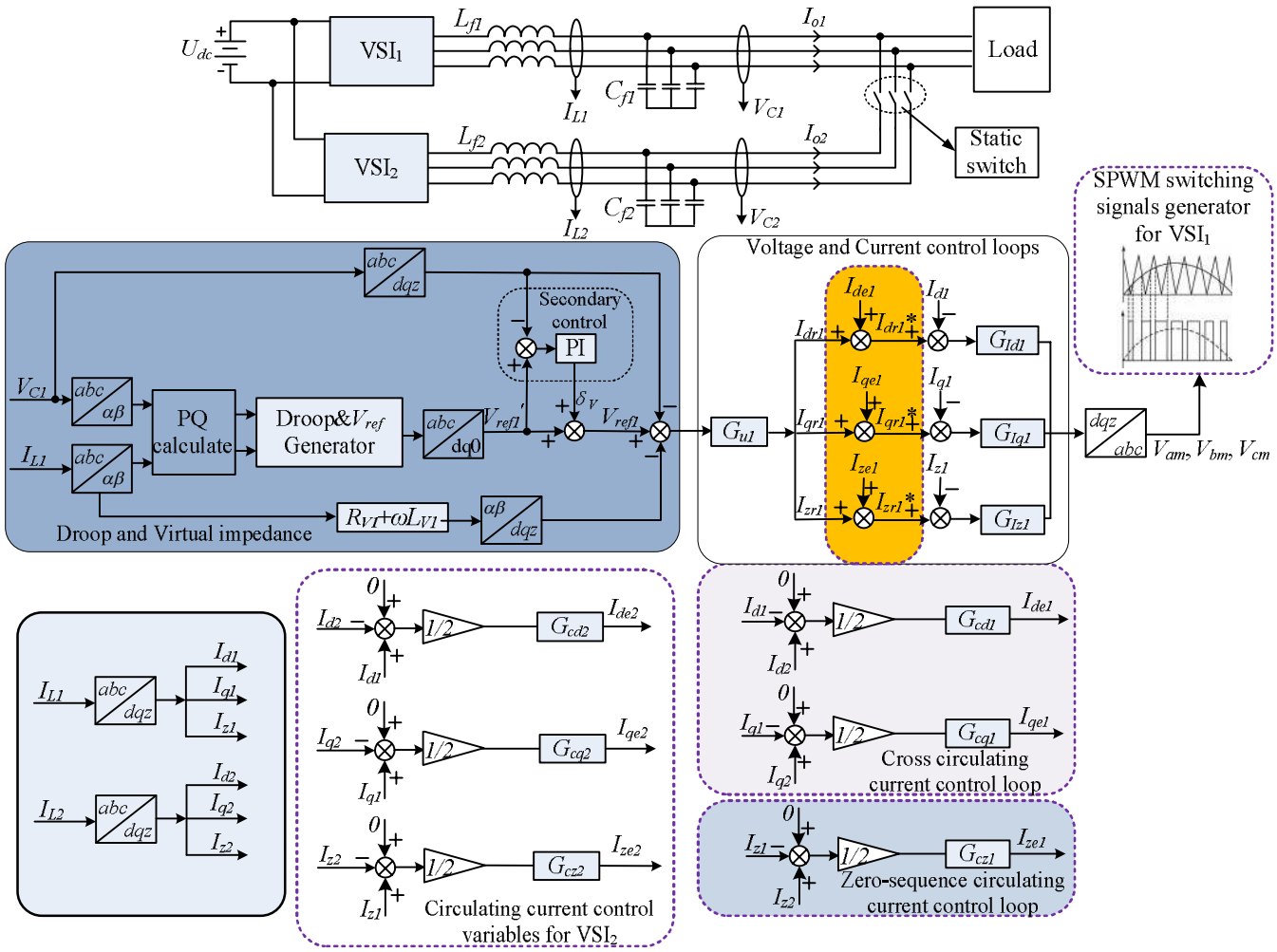

Fig. 4. The control scheme of parallel VSIs.

III. Influence Analysis of the Proposed Circulating-Current Control Loop

In order to analyze the influence and parameters sensitivity of the additional circulating-current control loop, a continuous model by using the transfer function of the control method has been developed in this paper. With the pole map of the characteristic equation, one can analyze the stability of the system and obtain the stability range of the control parameters.

The purpose of this paper is to present a circulating current suppression method to get a better current sharing performance for the existing control strategies. From Fig. 4, one can notice that, the output values of the circulating-current control loops are added to the original current loops. The basic control structure of the droop plus virtual impedance loop, and the secondary control will not be changed. Some previous works discussed the stability of control framework based on droop control plus the virtual impedance loop [34]–[41], while this paper puts more emphasis on analyzing the influence of the additional circulating-current control loop to the output voltage control. The reason of this is that since except the output impedance, the voltage difference among the inverters is another important issue that may cause circulating-currents which can also be seen from the circulating-current calculation equation (2) in Section II.A. Meanwhile, the conventional voltage and current controls will be compared with the proposed control method to illustrate more clearly the difference between them.

A. Analysis of Conventional Voltage and Current Control

The linear control model of conventional voltage and current control is shown in Fig. 5. Typically, it contains the model of control part and the model of power plant part. In the control part, $G_V(s)$ and $G_I(s)$ represent the voltage controller and current controller respectively. And in the power plant part, K_{PWM} represents the model of the inverter and it can be expressed as (20) in which T_S is the sampling time [38], rL represents the parasitic resistance of the output line, and it is determined by the equivalent series resistance (ESR) of the filter inductor and other parasitic elements. So the rL is not easy to measure or estimate [41].

$$K_{PWM} = 1/(1+1.5T_S) \tag{20}$$

Defining that:

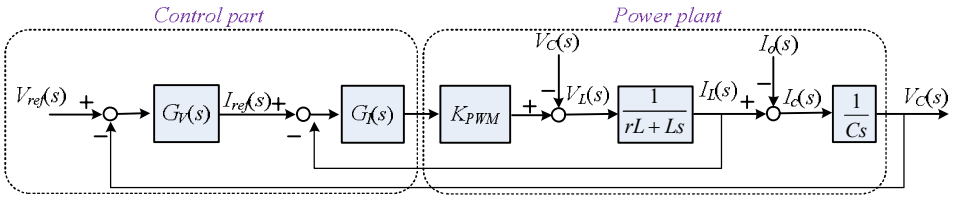

Fig. 5. Linear control model of conventional voltage and current control.

$$G_I(s) = K_{PI}\,,\ G_V(s) = K_{PV} + \frac{K_{IV}}{s} \tag{21}$$

and based on Fig. 5, one can deduce the close loop transfer function of the conventional voltage and current control as:

$$V_C(s) = \frac{K_{PV}K_{PI}K_{PWM}s + K_{PI}K_{IV}K_{PWM}}{D_1(s)}V_{ref}(s) - \frac{Ls^2 + (rL + K_{PI}K_{PWM})s}{D_1(s)}I_o(s) \tag{22}$$

where $D_1(s)$ is the characteristic equation expressed as

$$D_1(s) = LCs^3 + (rL + K_{PI}K_{PWM})Cs^2 + (K_{PV}K_{PI}K_{PWM} + 1)s + K_{PI}K_{IV}K_{PWM} \tag{23}$$

So that, if the parameters of the voltage/current control loops and the power plant are obtained, based on the pole map of $D_1(s)$, one can analyze the stability of the system.

Table I shows the parameters of the filter and controllers used in the experiments of this paper, in which rL=0.2Ω is considered as the ESR of the filter inductor, and K_{PWM} is considered as K_{PWM}≈1 since the T_S is very small under high switching frequency. By substituting the parameters into (23), one can get the following characteristic equation:

$$D_1(s) = 4.86e^{-8}s^3 + (5.4e^{-6} + 2.7e^{-5}K_{PI})s^2 + (1 + 1.5K_{PI})s + 10K_{PI} \tag{24}$$

By using the pole map analysis tool in Matlab, with the increase of K_{PI} from 1 to 20, and the increment step of 1, one can obtain the pole map as shown in Fig. 6. It is obviously that all the poles are located in the left filed of imaginary axis, which indicates that the system is stable with these controller parameters.

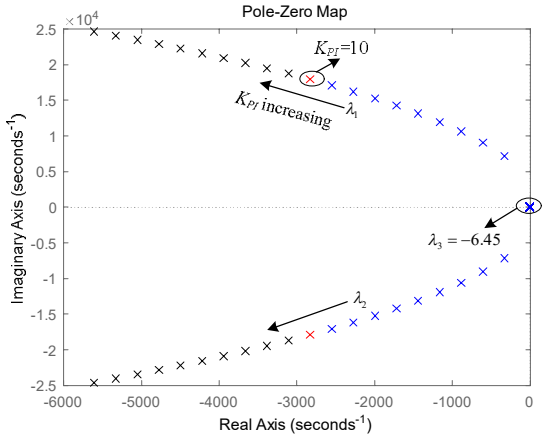

Fig. 6. Pole map with variable proportional part of current controller.

TABLE I
PARAMETERS OF FILTER AND CONTROLLERS WITH VARIABLE PROPORTIONAL CURRENT CONTROLLER

Coefficient	L	C	K_{PV}	K_{IV}	K_{PI}	rL
Value	1.8mH	27μF	1.5	10	1-20	0.2Ω

B. Model of Proposed Control Method

In order to analyze the transfer function of the proposed circulating current control loop in a simple way, the current control loop with circulating-current control will be introduced first, then it will be combined in the analysis of the voltage control loop.

Fig. 7 shows the linear control model of the current control loop with the proposed circulating current control loop. Compared with Fig. 5, there is one more variable $I_e(s)$ added to the original current reference $I_{ref}(s)$ to get a new current reference I_{ref}*(s). And $I_e(s)$ comes from the circulating-current control loop, which is the compensation value to suppress the circulating-current. From Fig. 7, one can obtain

$$I_{ref}{}^*(s) = I_{ref}(s) + I_e(s) \tag{25}$$

$$I_e(s) = \frac{1}{2}[0 - (I_{L1}(s) - I_{L2}(s))]G_C(s) \tag{26}$$

where $G_C(s)$ represents the controller of the circulating-current control loop. Substituting (26) into (25), and based on Fig. 7, one can deduce the transfer function as

$$I_{L1}(s)\bullet(Ls + rL) = \left\{I_{ref}(s) + \frac{1}{2}[(I_{L2}(s) - I_{L1}(s)]G_C(s) - I_{L1}(s)\right\} \bullet G_I(s)K_{PWM} - V_C(s) \tag{27}$$

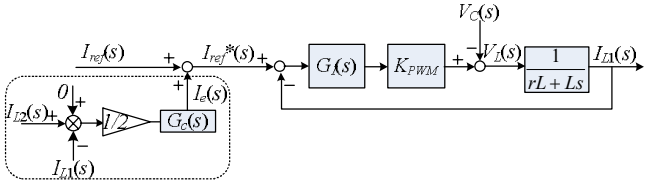

Fig. 7. Linear control model of current control loop with circulating-current control loop.

Furthermore, one can obtain (28) from (27), it depicts the influence of the reference current $I_{ref}(s)$, the capacitor voltage $V_C(s)$ and the inductor current $I_{L2}(s)$ from the neighbor inverter to the local inductor current $I_{L1}(s)$.

$$I_{L1}(s) = F_1(s)I_{ref}(s) + F_2(s)I_{L2}(s) - F_3(s)V_C(s) \tag{28}$$

In (28):

$$F_1(s)=\frac{G_I(s)K_{PWM}}{Ls+rL+[1+\frac{1}{2}G_C(s)]G_I(s)K_{PWM}} \tag{29}$$

$$F_2(s)=\frac{\frac{1}{2}G_C(s)G_I(s)K_{PWM}}{Ls+rL+[1+\frac{1}{2}G_C(s)]G_I(s)K_{PWM}} \tag{30}$$

$$F_3(s)=\frac{1}{Ls+rL+[1+\frac{1}{2}G_C(s)]G_I(s)K_{PWM}}. \tag{31}$$

Fig. 8 shows the control scheme of voltage control loop considering (28) and the proposed circulating-current control loop. Compared with the conventional voltage and current control, there is one more input named $I_{L2}(s)$.

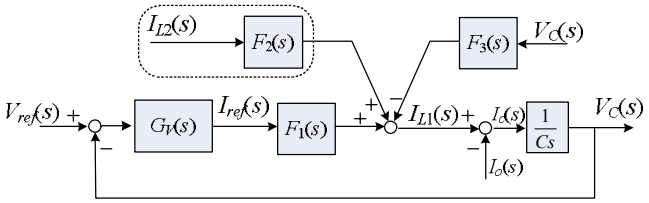

Fig. 8. Linear control model of the proposed voltage and current control.

From Fig. 8, one can deduce the transfer function which describes the influence of the reference voltage $V_{ref}(s)$, capacitor voltage $V_C(s)$ and the inductor current $I_{L2}(s)$ of the parallel-connected inverter to the output voltage:

$$\begin{aligned}V_C(s)=\{&[V_{ref}(s)-V_C(s)]G_V(s)F_1(s)+F_2(s)I_{L2}(s)\\&-F_3(s)V_C(s)-I_o(s)\}\frac{1}{Cs}\end{aligned} \tag{32}$$

Substituting (21), (29), (30) and (31) into (32), one can obtain:

$$\begin{aligned}V_C(s)=&\frac{2K_{PI}K_{PWM}(K_{PV}s+K_{IV})}{D_2(s)}V_{ref}(s)\\&+\frac{G_C(s)K_{PI}K_{PWM}s}{D_2(s)}I_{L2}(s)\\&-\frac{2Ls^2+\{2rL+[2+G_C(s)]K_{PI}K_{PWM}\}s}{D_2(s)}I_o(s)\end{aligned} \tag{33}$$

In which:

$$\begin{aligned}D_2(s)=&2LCs^3+\{2rL+[2+G_C(s)]K_{PI}K_{PWM}\}Cs^2\\&+2(K_{PV}K_{PI}K_{PWM}+1)s+2K_{PI}K_{IV}K_{PWM}\end{aligned} \tag{34}$$

Compared with the traditional voltage and current control, the main difference is that the influence of the inductor current from the neighbor inverter to the output voltage of local inverter is considered in the proposed control method.

The $D_2(s)$ in (34) is the characteristic equation, and $G_C(s)$ is the controller of the circulating-current control loop. The circulating-current controller $G_C(s)$ can be chosen as a PI controller as ($K_{PC}+K_{IC}/s$), or a P controller as K_{PC}. Then $D_2(s)$ can be written as

$$D_2(s)=a_0s^3+a_1s^2+a_2s+a_3. \tag{35}$$

The parameters of the coefficients a_0, a_1, a_2, and a_3 are listed in Table II.

TABLE II
COEFFICIENTS OF THE CHARACTERISTIC EQUATION

Coefficient	P controller of $G_C(s)$	PI controller of $G_C(s)$
a_0	$2LC$	$2LC$
a_1	$[2rL+(2+K_{PC})K_{PI}K_{PWM}]C$	$[2rL+(2+K_{PC})K_{PI}K_{PWM}]C$
a_2	$2(1+K_{PV}K_{PI}K_{PWM})$	$2(1+K_{PV}K_{PI}K_{PWM})$ $+K_{PI}K_{PWM}K_{IC}C$
a_3	$2K_{PI}K_{PWM}K_{IV}$	$2K_{PI}\bullet K_{PWM}\bullet K_{IV}$

Fig. 9 shows the pole map using the controller parameters shown in Table III. In Fig. 10, λ_i (i=1, 2, 3) represents the eigenvalues of the characteristic equation. With the increasing of the proportional parameter of the circulating-current controller K_{PC}, from 1 to 20 with increment step of 1, the eigenvalues change from λ_i (i=1, 2) to λ_i^* (i=1, 2). It can be seen that there will be always an eigenvalue of $\lambda_3=-6.17$. So, all the poles of the close loop transfer function are located in the left filed of imaginary axis, so that the system will remain stable.

Fig. 10 shows the pole map when K_{PC} is fixed with parameters shown in Table IV. The eigenvalues are always located in the left side of imaginary axis. The location of the poles does not change much with the increasing of the integral parameter of the circulating-current controller. It means that the integral parameter barely has influence to the system stability. It also can be seen clearly from the expression of the eigenvalues for the P and PI circulating-current controller, only the third eigenvalues a_2 are slightly different. So that, for the circulating-current control loop, a proportional controller is chosen for the experiments.

TABLE III
PARAMETERS OF THE CONTROLLERS WITH VARIABLE PROPORTIONAL PART OF CIRCULATING-CURRENT CONTROLLER

Coefficient	K_{PV}	K_{IV}	K_{PI}	K_{IC}	K_{PC}	rL
Value	1.5	10	8	5	1-20	0.2

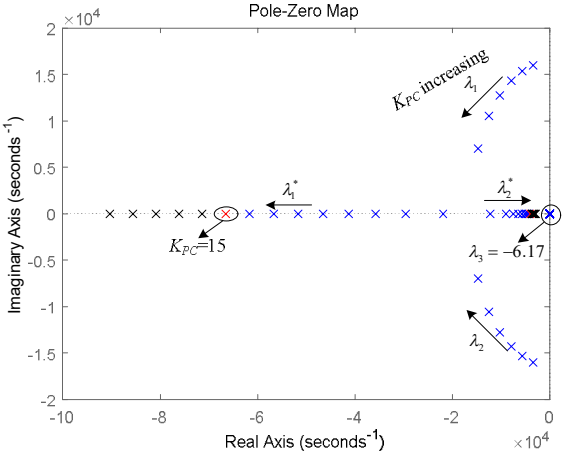

Fig. 9. Pole map when changing the proportional term value of the circulating-current controller.

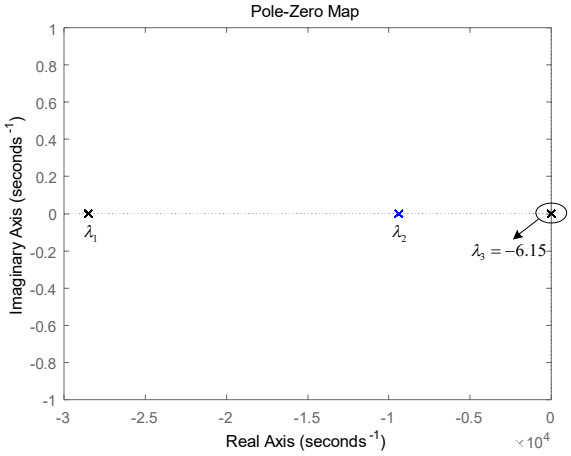

Fig. 10. Pole map when changing the integral term value of the circulating-current controller.

TABLE IV
PARAMETERS OF THE CONTROLLERS WITH VARIABLE INTEGRAL PART OF CIRCULATING-CURRENT CONTROLLER

Coefficient	K_{PV}	K_{IV}	K_{PI}	K_{IC}	K_{PC}	rL
Value	1.5	10	8	1-100	15	0.2

By analyzing the pole map of the transfer function of the proposed circulating-current control method with proper control parameters, one can guaranty the system stability.

C. The Selection of Virtual Impedance

The output impedance of the closed-loop inverter determines the droop control strategy [37]. The conventional droop scheme $P-\omega$ and $Q-V$ is often adopted. With the droop control, the frequency and the amplitude of the inverter output-voltage reference can be expressed as [37]:

$$\omega = \omega^* - m_p P \tag{36}$$

$$E = E^* - m_q Q \tag{37}$$

where ω^* and E^* are the output voltage reference frequency and amplitude, m_p and m_q are the droop coefficients. More details of droop control can be found in the literatures [40]–[43]. And for the conventional droop control scheme, a highly inductive output impedance at fundamental frequency is required to decouple the influence of P and Q to the frequency and voltage amplitude [42], [44].

Considering the transfer function (22) of the conventional voltage and current control, it can be written as (38) in which $G(s)$ can be seen as voltage gain and $Z_o(s)$ is the output impedance of the inverter [42], [44]. And the frequency-domain behavior of the output impedance can be analyzed through the Bode diagram [42].

$$V_C(s) = G(s)V_{ref}(s) - Z_o(s)I_o(s) \tag{38}$$

Considering virtual impedance in the voltage loop, $V_{ref}(s)$ in (38) should be replaced by $V_{ref}^*(s)$, in which $R_D(s)$ represents the virtual impedance.

$$V_{ref}^*(s) = V_{ref}(s) - R_D(s)I_o(s) \tag{39}$$

Supposing that the virtual impedance is chosen as (40), where R_V is the virtual resistance, and L_V is the virtual inductance.

$$R_D = R_V + sL_V \tag{40}$$

By deducing the transfer function of the output voltage with virtual impedance, one can obtain:

$$V_C(s) = \frac{K_{PV}K_{PI}K_{PWM}s + K_{PI}K_{IV}K_{PWM}}{D_1(s)}V_{ref}(s) - \frac{F_7(s)}{D_1(s)}I_o(s) \tag{41}$$

In which:

$$F_7(s) = (L + K_{PI}K_{PV}K_{PWM}L_V)s^2 + [rL + K_{PI}K_{PWM}(1 + K_{PV}R_V + K_{IV}L_V)]s + K_{PI}K_{IV}K_{PWM}R_V \tag{42}$$

With virtual impedance, the output impedance can be expressed as (43), in which $D_1(s)$ is as same as (22).

$$Z_o(s) = F_7(s)/D_1(s) \tag{43}$$

So that if the parameters of the power plant and the controller are obtained, one can analyze the frequency-domain behavior of the output impedance by using Bode diagram. Through the frequency-domain behavior, one can chose a proper virtual impedance to have a highly inductive output impedance for the conventional droop control.

The Bode diagram of the output impedance with virtual impedance is shown in Fig. 11. Four different parameters of virtual inductance L_V are analyzed, they are 0.2mH, 0.5mH, 0.9mH and 1.8mH respectively, and the virtual resistance is fixed as R_V=0.1. The X_{LV}/X_{RV} ratio should be kept in mind to make sure a highly inductive virtual impedance is applied [43], [44]. From Fig.11, one can notice that with the increasing of L_V, the impedance angle of the output impedance is closer to 90° at fundamental frequency, which behaves as a highly inductive output impedance. So based on the frequency-domain behavior of the output impedance and experimental results, one can select the virtual impedance. More details of the virtual impedance design and droop control can be found in literatures [40]–[44].

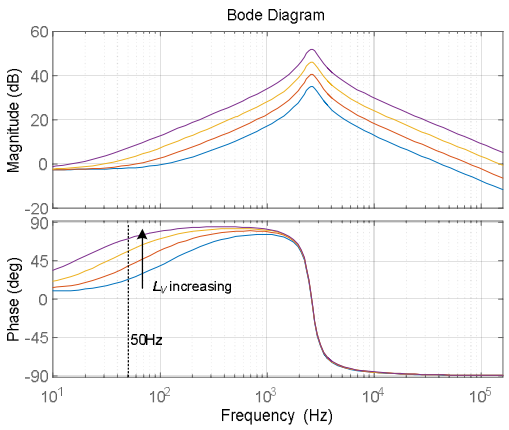

Fig. 11. Bode diagram of the output impedance considering virtual impedance, for L_V=0.2, 0.5, 0.9 and 1.8 mH (arrow direction indicates increasing value of L_V).

IV. Experimental Results

In order to verify the effectiveness of the proposed circulating-current control strategy, experiments were performed with a dSPACE 1006 system and two 2.2kVA three-phase two-level inverters from Danfoss. The parameters of the controllers and the power stage are shown in Table V and Table VI respectively.

TABLE V
PARAMETERS OF THE CONTROLLERS

Parameters	Value
Voltage controller	K_{PV}=1.5, KIV=10
Current controller	K_{PI}=8
Circulating-current controller	K_{PC}=15
R_{V1}, L_{V1}	0.1Ω, 0.9mH
R_{V2}, L_{V2}	0.15Ω, 0.9mH
droop coefficients	m_P=0.0001, m_q=0.0001

TABLE VI
PARAMETERS OF THE POWER STAGE

Parameters	Value
Linear load current	5.4A
Linear load power	3.7kVA
Nonlinear load peak current	9.4A
Nonlinear load configuration	3ϕ rectifier connected with a resistor (60Ω) and a capacitor (235μF)
Switching frequency	10kHz
Load voltage (RMS)	230V/50Hz
Filter inductances	C_{f1}=C_{f2}=27μF
Filter capacitances	L_{f1}=L_{f2}=1.8mH

Experimental results are shown below. Figs.12 to 18 are the experimental results when the linear load was connected. Figs. 19 to 26 are the experimental results when nonlinear load was sharing.

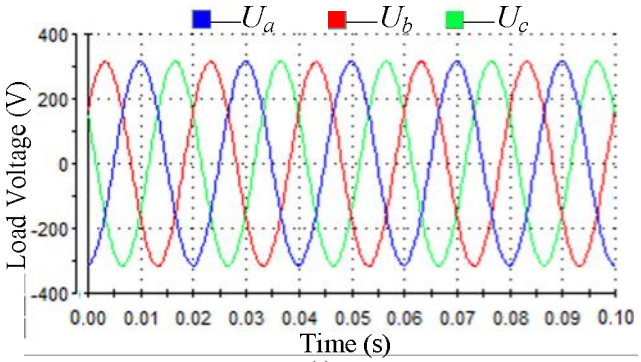

(a)

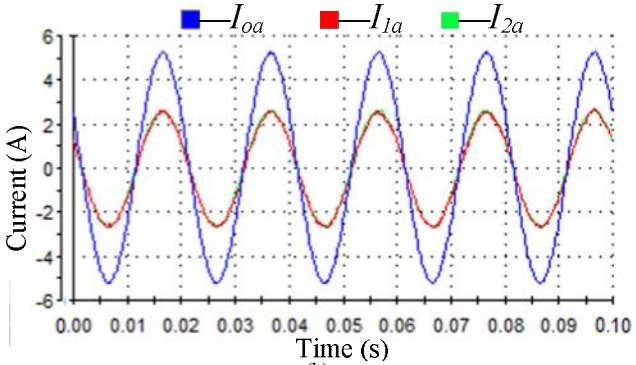

(b)

Fig. 12. Experimental results with the proposed control strategy when linear load is connected. (a) Load voltage. (b) Phase A currents of two inverters and the load.

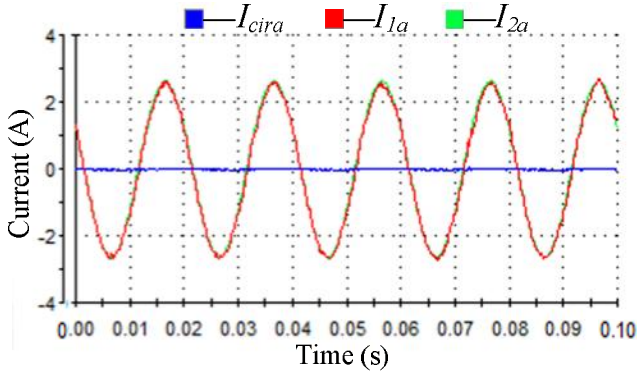

Fig. 13. The phase A output currents and cross circulating-current with the proposed circulating-current control loop when sharing linear load.

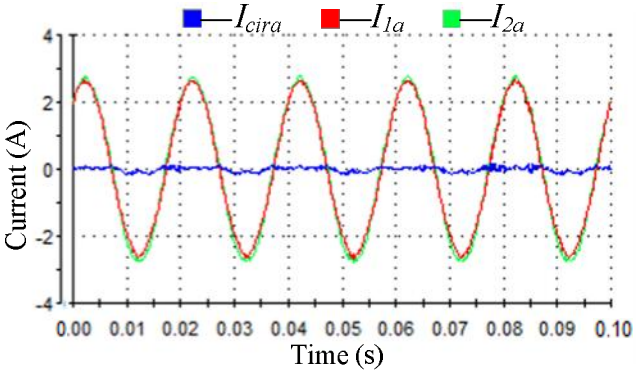

Fig. 14. The phase A output currents and cross circulating-current with the conventional droop plus virtual impedance control when sharing linear load.

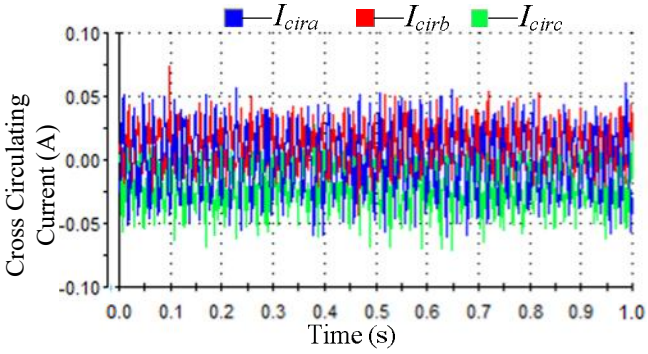

Fig. 15. The zoomed-in cross circulating-current with the proposed circulating-current control loop when sharing linear load.

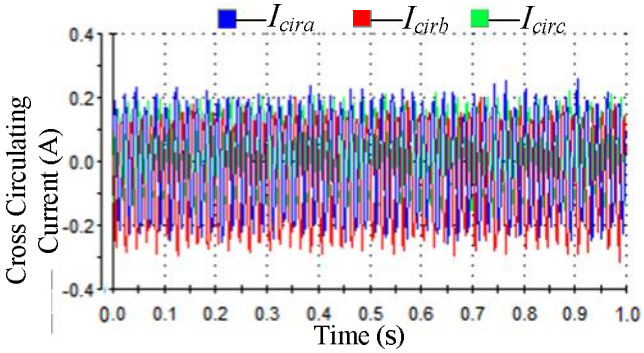

Fig.16. The zoomed-in cross circulating-current with the conventional droop plus virtual impedance control when sharing linear load.

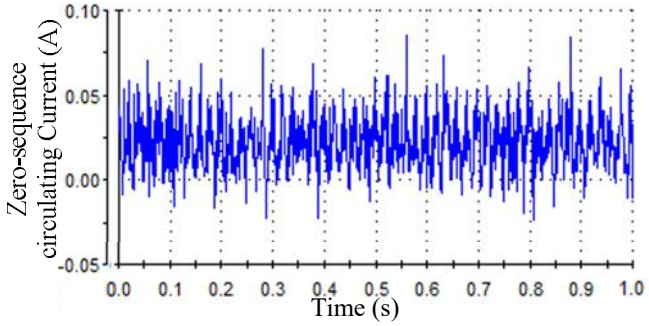

Fig.17. The zoomed-in zero-sequence circulating-current with the proposed circulating-current control loop when sharing linear load.

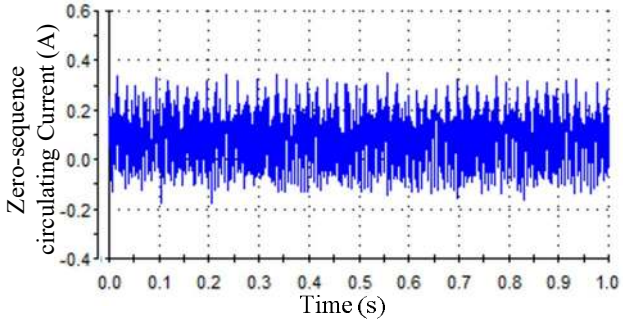

Fig.18. The zoomed-in zero-sequence circulating-current with the conventional droop plus virtual impedance control when sharing linear load.

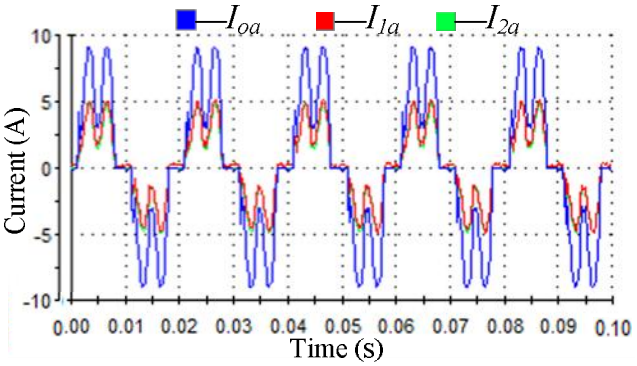

Fig. 19. The phase A output current and load current with the proposed circulating-current control loop when sharing nonlinear load.

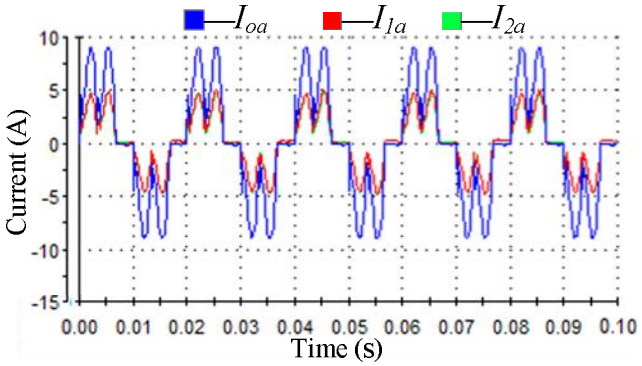

Fig. 20. The phase A output current and load current with the conventional droop plus virtual impedance control when sharing nonlinear load.

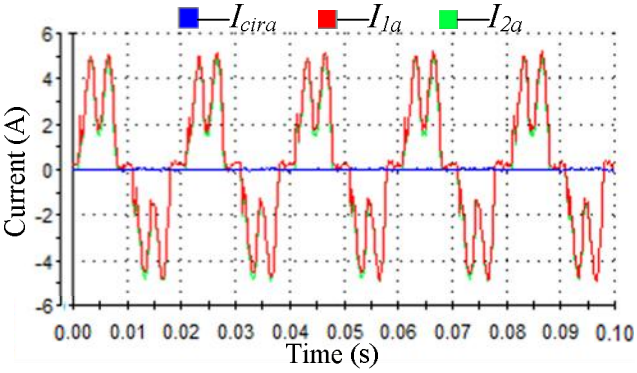

Fig. 21. The phase A output current and the cross circulating-current with the proposed circulating-current control loop when sharing nonlinear load.

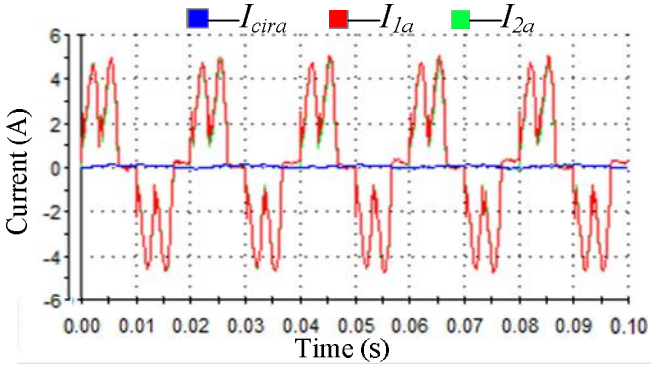

Fig. 22. The phase A current and the cross circulating-current with conventional droop plus virtual impedance control when sharing nonlinear load.

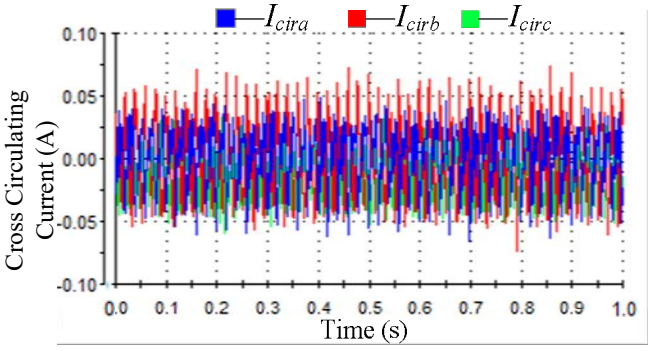

Fig. 23. The zoomed-in cross circulating-current with the proposed circulating-current control loop when sharing nonlinear load.

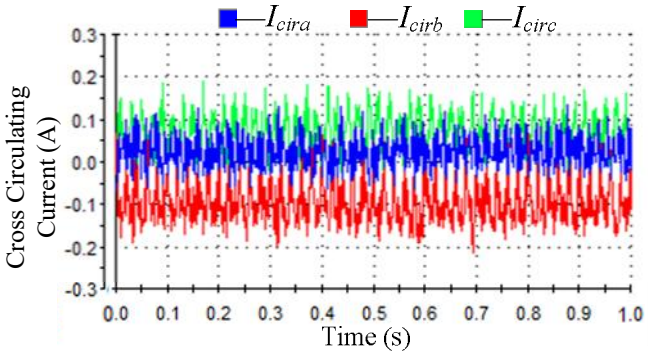

Fig. 24. The zoomed-in cross circulating-current with conventional droop plus virtual impedance control when sharing linear load.

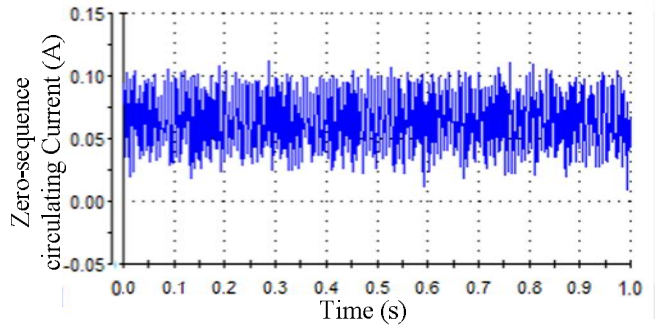

Fig. 25. The zoomed-in zero-sequence circulating-current with the proposed circulating-current control loop when sharing nonlinear load.

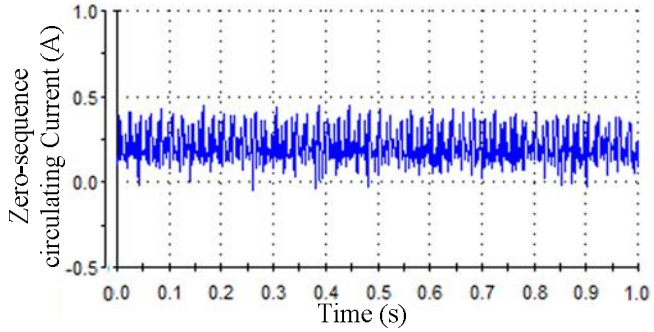

Fig. 26. The zoomed-in zero-sequence circulating-current with conventional droop plus virtual impedance control when sharing nonlinear load.

When linear load was sharing, from the experimental waveforms, one can notice that the peak value of the cross circulating-current and zero-sequence circulating-current are about 50mA and 75mA respectively with the proposed circulating-current control strategy. However, the values are about 200mA and 300mA when using the conventional droop plus virtual impedance control method.

More details about the obtained experimental results are shown in Table VII, which shows the approximate peak value of the circulating-currents. It can be seen that, independently from sharing linear or nonlinear loads, compared with the droop plus virtual impedance control, both of the cross circulating-current and the zero-sequence circulating-current can be effectively suppressed with the proposed control method. Thus a better performance of average current-sharing is realized.

TABLE VII
EXPERIMENTAL RESULTS COMPARISON (APPROXIMATE PEAK VALUE)

	Using the proposed control method		Using the conventional droop plus virtual impedance control	
	Linear load	Nonlinear load	Linear load	Nonlinear load
I_{cir}	50mA	75mA	200mA	200mA
I_{zcir}	75mA	100mA	300mA	400mA

V. CONCLUSION

Parallel-connected inverters systems are widely applied for high-power/high-reliable electrical supply requirements. In these systems, an accurate average current-sharing performance is necessary. In this paper, a circulating-current suppression method is proposed for paralleled VSIs with common AC and DC buses, which can be found in applications such as AC-DC hybrid microgrids and modular parallel UPS systems.

In the proposed approach, both of the cross and zero-sequence circulating-currents are considered and successfully suppressed. In comparison with the conventional droop plus virtual impedance control framework, it presents superior performances. The proposed concept to suppress the circulating-currents is based on the distributed control strategy. The system modeling is presented to study the influence of the additional circulating-current control loop to the output voltage. Then, the performance of the proposed control strategy is analyzed by using experimental results obtained from a parallel VSI system when sharing linear and nonlinear loads. The results demonstrate that the average current-sharing performance of the proposed control strategy is more accurate than that using the conventional droop plus virtual impedance control, pointing out that both of zero-sequence and cross circulating-currents among the parallel inverters can be effectively suppressed.

REFERENCES

[1] P. C. Loh, M. J. Newman, D. N. Zmood and D. G. Holmes, "A comparative analysis of multiloop voltage regulation strategies for single and three-phase UPS systems," *IEEE Trans. Power Electron*., vol. 18, no. 5, pp.1176–1185, Sept. 2003.

[2] X. Guo, "Three phase CH7 inverter with a new space vector modulation to reduce leakage current for transformerless photovoltaic systems," *IEEE Journal of Emerging and Selected Topics in Power Electronics.*, DOI: 10.1109/JESTPE.2017.2662015, 2017.

[3] X. Guo, W. Liu, and Z. Lu, "Flexible power regulation and current-limited control of grid-connected inverter under unbalanced grid voltage faults," *IEEE Trans. Ind. Electron*., DOI: 10.1109/TIE.2017.2669018, 2017.

[4] X. Guo, "A novel CH5 inverter for single-phase transformerless photovoltaic system applications," *IEEE Trans. Circuits and Systems II: Express Briefs*., DOI: 10.1109/TCSII.2017.2672779, 2017.

[5] X. Guo, and X. Jia, "Hardware-based cascaded topology and modulation strategy with leakage current reduction for transformerless PV systems," *IEEE Trans. Ind. Electron*., vol. 62, no. 12, pp. 7823–7832, Dec. 2016.

[6] R. Li, D. Xu, "Parallel Operation of Full Power Converters in Permanent-Magnet Direct-Drive Wind Power Generation System," *IEEE Trans. Ind. Electron*., vol. 60, no. 4, pp. 1619–1629, Apr. 2013.

[7] T. B. Lazzarin, G. A. T. Bauer, and I. Barbi, "A control strategy for parallel operation of single-phase voltage source inverters: Analysis, design and experimental result," *IEEE Trans. Ind. Electron*., vol. 60, no. 6, pp. 2194–2204, Jun. 2013.

[8] F. Wang, Y. Wang, Q. Gao, C. wang, and Y. liu, "A Control Strategy for Suppressing Circulating-currents in Parallel-Connected PMSM Drives with Individual DC Links," *IEEE Trans. Power Electron.*, vol. 31, no. 2, pp. 1680–1691, Feb. 2016.

[9] P. K. Goel, B. Singh, S. S. Murthy, and N Kishore, "Parallel operation of DFIGs in three-phase four-wire autonomous wind energy conversion system," *IEEE Trans. Ind. Appl.*, vol. 47, no. 4, pp. 1872–1883, Jul./Aug. 2011.

[10] D. C. Pham, S. Huang, and K. Huang, "Modeling and Simulation of Current Source Inverters with Space Vector Modulation," in *Proc. IEEE ICEMS.*, 2010, pp. 320–325.

[11] T. P. Chen, "Circulating zero-sequence current control of parallel three-phase inverters," in *Proc. Inst. Elect. Eng.—Elect. Power Appl.*, 2006, vol. 153, no. 2, pp. 282–288.

[12] L. Asiminoaei, E. Aeloiza, P. N. Enjeti, and F. Blaabjerg, "Shunt active-power-filter topology based on parallel interleaved inverters," *IEEE Trans. Ind. Electron*., vol. 55, no. 3, pp. 1175–1189, Mar. 2008.

[13] Y. Chen and K. M. Smedley, "One-cycle-controlled three-phase grid-connected inverters and their parallel operation," *IEEE Trans. Ind. Appl.*, vol. 44, no. 2, pp. 663–671, Mar./Apr. 2008.

[14] R. M. Cuzner, D. J. Nowak, A. Bendre, G. Oriti, and A. L. Julian, "Mitigating circulating common-mode currents between parallel soft-switched drive systems," *IEEE Trans. Ind. Appl*., vol. 43, no. 5, pp. 1284–1294, Sep./Oct. 2007.

[15] F. S. Pai, J. M. Lin, and S. J. Huang, "Design of an inverter array for distributed generations with flexible capacity operations," *IEEE Trans. Ind. Electron*., vol. 57, no. 12, pp. 3927–3934, Dec. 2010.

[16] T. Itkonen, J. Luukko, T. Laakkonen, P. Silventoinen, and O. Pyrhonen, "Switching effects in directly paralleled three-phase AC/DC/AC convert- ers with separate DC links," in *Proc. IEEE Power Electron. Spec. Conf*., 2008, pp. 1937–1943.

[17] X. Zhang, J. Chen, Y. Ma, Y. Wang, and D. Xu, "Bandwidth Expansion Method for Circulating-current Control in Parallel Three-phase PWM Converter Connection System," *IEEE Trans. Power Electron*., vol. 29, no. 12, pp. 6847–6856, Dec. 2014.

[18] J. K. Ji and S. K. Sul, "Operation analysis and new current control of parallel connected dual converter system without interphase reactors," in *Proc. 25th Annu. Conf. Ind. Electron. Soc*., San Jose, America, 1999, pp. 235–240.

[19] T. P. Chen, "Zero-Sequence Circulating-current Reduction Method for Parallel HEPWM Inverters Between AC Bus and DC Bus," *IEEE Trans. Ind. Electron*., vol. 59, no. 1, pp. 290–300, Jan. 2012.

[20] C. T. Pan and Y. H. Liao, "Modeling and coordinate control of circulating-currents in parallel three-phase boost rectifiers," *IEEE Trans. Ind. Electron*., vol. 54, no. 2, pp. 825–838, Apr. 2007.

[21] M. Jones, S. N. Vukosavic, and E. Levi, "Parallel-connected multiphase multidrive systems with single inverter supply," *IEEE Trans. Ind. Electron*., vol. 56, no. 6, pp. 2047–2057, Jun. 2009.

[22] Z. H. Ye, D. Boroyevich, J. Y. Choi, and F. C. Lee, "Control of circulating-current in two parallel three-phase boost rectifiers," *IEEE Trans. Power Electron*., vol. 17, no. 5, pp. 609–615, Sep. 2002.

[23] K. Xing, F. C. Lee, D. Borojevic, Z. H. Ye, and S. Mazumder, "Interleaved PWM with discontinuous space-vector modulation," *IEEE Trans. Energy Convers*., vol. 14, no. 5, pp. 906–917, Sep. 1999.

[24] J. M. Guerrero, J. Matas, L. G. Vicuna, M. Castilla, and J. Miret, "Wireless-control strategy for parallel operation of distributed-generation inverters," *IEEE Trans. Ind. Electron*., vol. 53, no. 5, pp. 1461–1470, Oct. 2006.

[25] Y. Zhang, M. Yu, F. Liu, and Y. Kang, "Instantaneous Current-Sharing Control Strategy for Parallel Operation of UPS Modules Using Virtual Impedance," *IEEE Trans. Power Electron*., vol. 28, no. 1, pp. 432–440, Jan. 2013.

[26] J. M. Guerrero, L. G. Vicuna, J. Matas, M. Castilla, and J. Miret, "Output impedance design of parallel-connected UPS inverters with wireless load-sharing control," *IEEE Trans. Ind. Electron*., vol. 52, no. 4, pp. 1126–1135, Aug. 2005.

[27] J. He, and Y. Li, "Analysis, Design, and Implementation of Virtual Impedance for Power Electronics Interfaced Distributed Generation," *IEEE Trans. Ind. Applica*., vol. 47, no. 6, pp. 2525–2538, Nov. 2011.

[28] B. Wei, J. C. Vasquez, J. M. Guerrero, and X. Guo, "Control architecture for paralleled current-source-inverter (CSI) based uninterruptible power systems (UPS)," in *Proc. IEEE IPEMC-ECCE Asia*., 2016, pp. 151–156.

[29] B. Wei, J. M. Guerrero, J. C. Vasquez, and X. Guo, "A Circulating-current Suppression Method for Parallel Connected Voltage-Source-Inverters (VSI) with Common DC and AC Buses," in *Proc. IEEE Energy Conversion Congress and Exposition (ECCE)*., 2016., DOI: 10.1109/ECCE.2016.7854655, pp. 1–6.

[30] M. Prodanovic, T.C. Green, and H. Mansir, "Survey of control methods for three-phase inverters in parallel connection," in *Proc. 8th Int. Conf. on Power Electron. and Variable Speed Drives.*, 2000, pp. 472–477.

[31] H. Cai, R. Zhao, and H. Yang, "Study on Ideal Operation Status of Parallel Inverters," *IEEE Trans. Power Electron*., vol. 23, no. 6, pp. 2964–2969, Nov. 2008.

[32] B. Li, C. Wang, "Comparative analysis on PMSM control system based on SPWM and SVPWM," in *Proc. Chinese Control and Decision Conference* (*CCDC*)., 2016, pp. 5071–5075.

[33] J. Sabarad; G. H. Kulkarni, "Comparative Analysis of SVPWM and SPWM Techniques for Multilevel Inveter," in *Proc. International Conference on Power and Advanced Control Engineering* (*ICPACE*)., 2015, pp. 232–237.

[34] E. A. Coelho, P. C. Cortizo, and P. F. Garcia, "Small-Signal Stability for Parallel-Connected Inverters in Stand-Alone AC Supply Systems," *IEEE Trans. Ind. Appl*., vol. 38, no. 2, pp. 533–542, Mar./Apr. 2002.

[35] E. Barklund, N. Pogaku, M. Prodanovic´, C. Hernandez-Aramburo, and T. C. Green, "Energy Management in Autonomous Microgrid Using Stability-Constrained Droop Control of Inverters," *IEEE Trans. Power Electron*., vol. 23, no. 5, pp. 2346–2352, Sep. 2008.

[36] Y. I. Mohamed and E. F. El-Saadany, "Adaptive Decentralized Droop Controller to Preserve Power Sharing Stability of Paralleled Inverters in Distributed Generation Microgrids," *IEEE Trans. Power Electron.*, vol. 23, no. 6, pp. 2806–2816, Nov. 2008.

[37] E. A. Coelho, D. Wu, J. M. Guerrero, J. C. Vasquez, T. Dragičević, Č. Stefanović, and P. Popovski, "Small-Signal Analysis of the Microgrid Secondary Control Considering a Communication Time Delay," *IEEE Trans. Ind. Electron*., vol. 63, no. 10, pp. 6257–6269, Oct. 2016.

[38] X. Wang, F. Blaabjerg and Z. Chen, "An Improved Design of Virtual Output Impedance Loop for Droop-Controlled Parallel Three-Phase Voltage Source Inverters," in *Proc. IEEE Energy Conversion Congress and Exposition* (*ECCE*)., 2012, pp. 2466–2473.

[39] X. Wang, Y. Li, F. Blaabjerg, and P. C. Loh, "Virtual-Impedance-Based Control for Voltage-Source and Current-Source Converters," *IEEE Trans. Power Electron*., vol. 30, no. 12, pp. 7019–7037, Dec. 2015.

[40] J. Matas, M. Castilla, L. Vicuña, J. Miret, and J. C. Vasquez, "Virtual Impedance Loop for Droop-Controlled Single-Phase Parallel Inverters Using a Second-Order General-Integrator Scheme," *IEEE Trans. Power Electron*., vol. 25, no. 12, pp. 2993–3001, Dec. 2010.

[41] J. C. Vasquez, J. M. Guerrero, M. Savaghebi, J, Eloy-Garcia, and R. Teodorescu, "Modeling, Analysis, and Design of Stationary Reference Frame Droop Controlled Parallel Three- Phase Voltage Source Inverters," *IEEE Trans. Ind. Electron*., vol. 60, no. 4, pp. 1271–1280, Apr. 2013.

[42] J. M. Guerrero, L. G. Vicuña, J. Matas, M. Castilla, and J. Miret, "Output Impedance Design of Parallel-Connected UPS Inverters With Wireless Load-Sharing Control," *IEEE Trans. Ind. Electron*., vol. 52, no. 4, pp. 1126–1135, Aug. 2005.

[43] J. M. Guerrero, J. C. Vasquez, L. G. Vicuña, and M. Castilla, "Hierarchical Control of Droop-Controlled AC and DC Microgrids—A General Approach Toward Standardization," *IEEE Trans. Ind. Electron*., vol. 58, no. 1, pp. 158–172, Jan. 2011.

[44] S. Xu and J. Xu, "Parallel Control Strategy of Single-Phase Inverter Based on Virtual Impedance," in *Proc. International Conference on Communications, Circuits and Systems* (*ICCCAS*)., 2010, pp. 589–592.